Global and Planetary Change 228 (2023) 104203

Contents lists available at ScienceDirect

Global and Planetary Change

journal homepage: www.elsevier.com/locate/gloplacha

Climate change has enhanced the positive contribution of rock weathering to the major ions in riverine transport

Suhua Gong [a,b], Xiaoyong Bai [a,c,e,*], Guangjie Luo [d], Chaojun Li [a,b], Luhua Wu [a,b], Fei Chen [a,b], Chen Ran [a,b], Huipeng Xi [a,b], Sirui Zhang [a,b]

[a] State Key Laboratory of Environmental Geochemistry, Institute of Geochemistry, Chinese Academy of Sciences, Guiyang 550081, Guizhou Province, China
[b] University of Chinese Academy of Sciences, Beijing 100049, China
[c] College of Resources and Environmental Engineering, Guizhou University, Guiyang 550025, China
[d] Guizhou Provincial Key Laboratory of Geographic State Monitoring of Watershed, Guizhou Education University, Guiyang 550018, China
[e] CAS Center for Excellence in Quaternary Science and Global Change,Xi'an, 710061,Shanxi Province,China

ARTICLE INFO

Editor: Dr. Alan Haywood

Keywords:
Ions
Chemical weathering of rocks
Climate change
Controlling factors
Vegetation response

ABSTRACT

Most of the ions in rivers come from the migration of weathering products of continental rocks. However, there is no clear understanding of the dynamic changes in ions derived from the chemical weathering of rocks and their feedback to climate change. This affects our comprehension of the evolution of life and the cycle of matter on Earth. In the present study, we established a dataset with a 0.25° × 0.25° spatial resolution for the major dissolved ions and their total fluxes in the riverine transported (ICWR) at the global scale from 1980 to 2020 using the Lechuga-Crespo model and the random forest algorithm. The results show that from 1980 to 2009, the total amount of the ICWR was $5.4{\cdot}10^9$ Mg yr^{-1}, of which alkalinity accounted for 45%, Ca^{2+} accounted for 17%, SO_4^{2-} accounted for 14%, Na^+ accounted for 9%, Cl^- accounted for 8%, Mg^{2+} accounted for 6%, and K^+ accounted for 2%. In addition, the ICWR increased at a rate of $6.47{\cdot}10^6$ Mg yr^{-1}. The most obvious trend was in the area with high ionic activity coefficients between 30° N and 30° S. The growth trend of the ICWR during 2010–2020 was seven times that during 1980–2009, resulting in a 30% increase in the ICWR over the past 40 years. This study highlights the critical role of climate change in the transport and evolution of the ICWR, and explores their impact on vegetation change. It has important reference value for responding to the eco-environmental problems caused by climate change.

1. Introduction

As an important carrier of material circulation and energy transfer between land and sea, rivers are not only an important part of the global water cycle but also a key link in the global carbon cycle (Gaillardet et al., 1999; Hindshaw et al., 2011; Relph et al., 2021; Liu et al., 2023). Rivers transport the products of surface processes to the ocean in the process of shaping landforms (Sarin and Krishnaswami, 1984; Navarre-Sitchler and Thyne, 2007; Patel et al., 2020). Their solute loads and chemical compositions reflect the characteristics of their basins' geomorphic evolution, hydrological cycles, eco-environmental changes, and human activities (Stallard and Edmond, 1983; Meybeck, 2003; Liu and Han, 2020; Kemeny et al., 2021; Liu et al., 2022). The solutes in rivers may come from natural factors such as rock weathering, soil erosion, atmospheric deposition, and glacier melting, or from human factors such as industrial, agricultural, and domestic sewage discharge (Roy et al., 1999; Ruan et al., 2019; Li et al., 2022; Ran et al., 2023). In addition, their hydrochemical characteristics are mainly influenced by the basin lithology, meteorological and hydrological conditions, vegetation cover, and human activities (Moon et al., 2007; Zhang et al., 2015).

Since the 20th century, scholars have carried out extensive research on river hydrochemistry in the major basins of the world's continents and have explored the main controlling factors and response mechanisms (Sioli, 1968; Gibbs, 1970; Liu et al., 2018; Luo, 2022; Xiao et al., 2023). The chemical weathering of rocks provides the material source for the ions in rivers, and their carbon sink effect is a key component of the global carbon cycle (Walker et al., 1981; Li et al., 2018; Xi et al., 2021; Bai et al., 2023; Xu et al., 2024). Previous studies have demonstrated that the chemical weathering of rocks has a sensitive feedback

* Corresponding author at: Institute of Geochemistry, Chinese Academy of Sciences, 99 Lincheng West Road, Guiyang 550081, Guizhou Province, China.
E-mail address: baixiaoyong@vip.skleg.cn (X. Bai).

https://doi.org/10.1016/j.gloplacha.2023.104203
Received 18 February 2023; Received in revised form 18 July 2023; Accepted 21 July 2023
Available online 30 July 2023

effect on climate change (Gislason et al., 1996; Beaulieu et al., 2012; Tipper et al., 2012; Gong et al., 2020). Due to the increasing amount of greenhouse gases produced since the Industrial Revolution (Vitousek, 1994; Cox et al., 2000), global warming has now reached 1.2 °C and is expected to increase to 1.5 °C above pre-industrial levels by 2030–2052 (National Climate Center, 2021; IPCC, 2018). Global warming not only accelerates the rate of the chemical weathering of rocks, but it also causes changes in the total content of ions derived from the chemical weathering of rocks in riverine transport. However, there is still a lack of research on the temporal and spatial evolution, controlling factors, response to climate change and ecological environment effects of the ions derived from the chemical weathering of rocks on grid cell scale. Therefore, revealing the influence of global warming on the chemical weathering of rocks through the dissolved ions changes is an important new direction in global research. At the same time, vegetation has a high sensitivity to changes in the concentration of elements required for its growth, so changes in ion concentrations in rivers caused by climate change will also affect the growth of vegetation. An appropriate concentration of ions can promote the growth of vegetation. When the ion concentration is too low or too high, it will have a negative impact on the growth and development of vegetation (Ye et al., 2010; Hawkesford et al., 2012). Hence. exploring the effect of the ions derived from the chemical weathering of rocks on vegetation changes is not only the theoretical basis for analyzing vegetation growth differences, but also can provide new ideas for promoting global vegetation greening and improving the carbon sequestration efficiency of ecosystems.

Thus, using the Lechuga-Crespo model (Lechuga-Crespo et al., 2020) and the random forest algorithm, we first created a dataset with a spatial resolution of 0.25° × 0.25° for the major ions derived from the chemical weathering of rocks (ICWR), i.e. Ca^{2+}, Mg^{2+}, K^{+}, Na^{+}, SO_4^{2-}, Cl^{-}, alkalinity (Here only represent HCO_3^{-} and CO_3^{2-}), and their total fluxes in the riverine transported ICWR at the global scale from 1980 to 2020. The objectives of this study were *i)* to complement the gaps in the ICWR dynamic spatial dataset; *ii)* to quantify the relative contribution rates of climate factors to the impact of the ICWR; *iii) to e*xplore the impact of ICWR on vegetation change. The ICWR calculation results based on the process model improve our understanding of the magnitude, spatial pattern, change trend, and controlling factors of global ICWR. Its response to climate change provides convincing evidence and data to support the development of a new ICWR-climate change feedback model. Under the continuing effects of climate change, the changes in ions will have a dramatic impact on the evolution of life and the various geochemical cycles, which highlights the importance of research on the relationship between the ICWR and climate change.

2. Materials and methods

2.1. Materials

The main ion sites in the river hydrochemistry database were obtained from the GLORICH database (Hartmann et al., 2014). In the database, we selected hydrochemical chemistry data from 9909 sampling locations between 1980 and 2009 and divided them into annual data according to the time of collection (Fig.S1). The soil database contained soil moisture (SM) and soil temperature data. The meteorological and hydrological database contained temperature (T), precipitation (P), evapotranspiration (ET), runoff (Q), nitrogen deposition (ND), partial pressure of carbon dioxide (PCO_2), and wind speed (WS) data. The vegetation database contained leaf area index and carbon mass by leaf and above-ground litterfall data. The human activity database mainly included land use data. Since the time series of land use data with a resolution of 300 m in the European Space Agency (ESA) Global Land Cover data (https://cds.climate.copernicus.eu/) were from 1982 to 2020, the land use data with a resolution of 0.25° × 0.25° in the Coupled Model Intercomparison Project Phase 6 (CMIP 6) (https://esgf-node.llnl.gov/search/cmip6/) from 1980 to 1991 were selected as supplementary data. The remaining data were from CMIP 6 and they were for the period 1980–2020 at a resolution of 25 km. The fractional vegetation cover (FVC) and the net primary productivity (NPP) data representing vegetation changes. The FVC data was obtained from products with a resolution of 0.5° × 0.5° in The Global Land Surface Satellite (GLASS), and the NPP data was obtained from products with a resolution of 0.0727° × 0.0727° from the National Science & Technology Infrastructure (Zhou et al., 2022). The resampling method was used to aggregate these data to a resolution of 0.25° × 0.25° to match the spatial resolution of each other. The lithology data were obtained from Hartmann's research (Hartmann and Moosdorf, 2012). The basin boundaries and climate zones were derived from the Global Runoff Data center (GRDC) (https://grdc.com.au/) database and the Köppen climate classification data (Beck et al., 2020).

The workflow followed is shown in Fig. 1. First, a random forest model was used to invert the data from the processed database to simulate the flux maps of the river ions on grid cell scale. Subsequently, flux maps of the ICWR were calculated using the Lechuga-Crespo model. Next, spatiotemporal evolution maps of the ICWR were obtained using the trend analysis method based on the pixels. On the one hand, the Lindeman-Merenda-Gold (LMG) model was used to quantify the relative contribution rate of climate change factors to ICWR, and on the other hand, the response of vegetation to ICWR changes was explored through partial correlation analysis.

2.2. Methods

2.2.1. Lechuga-Crespo model

Based on the factors influencing the chemical weathering rate of rocks, Lechuga-Crespo developed a model to calculate ICWR by adding explanatory variables to the model in the following order: lithology, soil shielding effect (Hartmann et al., 2014), temperature, hydraulic conductivity and soil depth. Then, the accuracy of ICWR results obtained from simulations of the model containing different variables was tested, and it was demonstrated that the simulation results of the following models using the corresponding variables had the highest accuracy (Lechuga-Crespo et al., 2020). This model was used to select the fraction of major ions in riverine that were derived from chemical weathering of the rocks, and it is expressed as follows:

$$F_x^* = q_{ann} \cdot f_{S_x}(soil) \cdot \sum (L_i \cdot C_{x_i}) \quad (1)$$

where F_x^* is the flux of ion x derived from chemical weathering of the rocks; q_{ann} is runoff; L_i is the area ratio occupied by lithology i; $f_{sx}(soil)$ is soil shielding effect, $f_{s\ ,\ Ca2+} = 0.75$, $f_{s\ ,\ Mg2+} = 0.74$, $f_{s\ ,\ Na+} = 0.46$, $f_{s\ ,\ K+} = 0.78$, $f_{s\ ,\ SO4-} = 0.29$, $f_{s\ ,\ Cl-} = 0.34$, $f_{s\ ,\ Alkalinity} = 0.70$; and C_{xi} is the average concentration of ion x draining from lithology i.

2.2.2. Random forest

The random forest algorithm is a machine learning algorithm based on a classifier ensemble and decision trees. The decision tree is modeled on the samples extracted using the bootstrap resampling and replacement method, and the unextracted samples from the control dataset. The randomForest package in R was used to construct a random forest model in this paper. The construction of a large number of decision trees increases the differences among the classification models and improves the extrapolation and prediction capabilities of the models. A simple majority voting method is used to determine the final classification, thus establishing a relationship between a dependent variable Y and several independent variables X without the occurrence of overfitting (Breiman, 1996; Breiman, 2001). The final classification decision-making principle is as follows (Fang et al., 2011):

$$H(x) = \underset{Y}{argmax} \sum_{i=1}^{k} I(h_i(x) = Y) \quad (2)$$

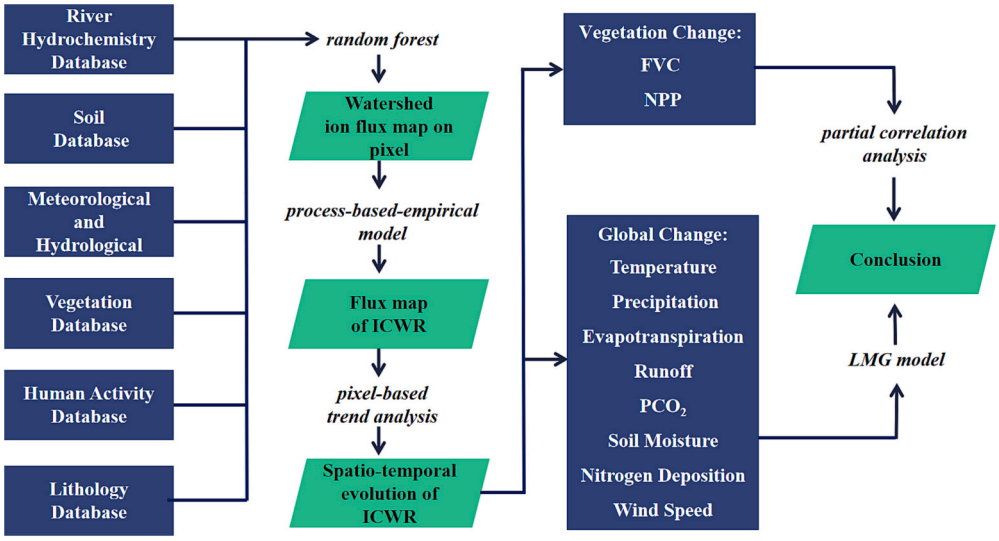

Fig. 1. Summary of the workflow. The white text in the blue box indicates data; the black italic text indicates the methods; and the black text in the green box indicates the results obtained. FVC is the fractional vegetation cover. NPP is the net primary productivity. (For interpretation of the references to colour in this figure legend, the reader is referred to the web version of this article.)

where $H(x)$ is the combined classification model, h_i is the decision tree classification model, $I(\cdot)$ is the indicator function, and Y is output variable.

Therefore, the extrapolation prediction ability of random forest model can be used to transform the site data into grid cell data by inversion. The site data of river hydrochemistry from GLORICH database, combined with data from other databases, can be simulated by random forest model to obtain spatial distribution maps of major ions in riverine on grid cell scale.

2.2.3. Trend analysis method

The pixel-based trend analysis method was used to analyze the evolution trend of the ICWR in a long time series. This method performs regression analysis of the ICWR with time as the independent variable, and the calculated slope θ is the evolution trend of the ICWR. $\theta < 0$ indicates that the ICWR on grid cell scale exhibits a decreasing trend, and vice versa. The slope θ is determined as follows (Sun and Guo, 2012):

$$\theta = \frac{n \times \sum_{i=1}^{n}(i \times F_{x_i}) - \left(\sum_{i=1}^{n} i\right)\left(\sum_{i=1}^{n} F_{x_i}\right)}{n \times \sum_{i=1}^{n} i^2 - \left(\sum_{i=1}^{n} i\right)^2} \tag{3}$$

where θ is the evolution trend, Fxi is the ion concentration in year i, n is the research period, and i indicates from 1 to n.

2.2.4. Lindeman-Merenda-Gold model

We quantified the contributions of the climate change factors to the multiple regression model of the ICWR based on the LMG model. The relative contribution rates of the factors introduced into the model to the ICWR were obtained by decomposing the dependent variable variance after de-averaging all of the possible marginal contributions of the variables. The correlation matrix diagram was drawn using a machine learning method and the generalized linear model of logistic regression. The formula for the LMG is as follows (Sen et al., 1981; Ulrike, 2006; Gong et al., 2020):

$$LMG(x_k) = \frac{1}{p!} \sum_{\substack{S \subseteq \{x_1, \cdots x_p\} \\ \{x_k\}}} n(S)!(p - n(S) - 1)! seqR^2(\{x_k\}|S) \tag{4}$$

where LMG is the expectation of the marginal contribution of regression variable x_k in all sequences, x is the individual regression factor, S is the variable set, and R^2 is the goodness-of-fit.

2.2.5. Partial correlation analysis

Partial correlation analysis was to analyze the correlation between two variables separately in multiple regression under the premise of excluding the interference of other variables, which can more accurately reflect their linear relationship. By comparing the correlation and partial correlation between ICWR and vegetation change, we obtained the difference of the effect of different ions on FVC and NPP. Partial correlation was calculated using the correlation matrix inversion method, and its logarithmic matrix is as follows (Duan and Zhang, 1992):

$$R = \begin{bmatrix} r_{11} & r_{12} & \cdots & r_{1n} \\ r_{21} & r_{22} & \cdots & r_{2n} \\ \cdots & \cdots & \cdots & \cdots \\ r_{n1} & r_{n2} & \cdots & r_{nn} \end{bmatrix} \tag{5}$$

where r is the correlation coefficient, n is the number of samples, x_i and y_i represent variable values. The formula for calculating the partial correlation coefficient is:

$$R_{ij} = \frac{-\triangle_{ij}}{\sqrt{\triangle_{ii} \cdot \triangle_{jj}}} \tag{6}$$

where R_{ij} is the partial correlation coefficient of variables x_i and y_i, Δ is the algebraic cofactor of the elements in the matrix.

3. Results

3.1. Global dynamic changes in the riverine transported ICWR from 1980 to 2009

3.1.1. Global distribution of the ICWR in riverine transport

The spatial distribution of the ICWR fluxes was strongly influenced by climate. From 1980 to 2010, except for the areas with no data, the areas with high ICWR total ion fluxes were mainly located in Southeast Asia, the Godavari Basin, the Yangtze River Basin, the southwestern edge of the Qinghai-Tibetan Plateau, the western part of the Andes Mountains, the Orinoco Basin, and the Amazon Basin (Fig. 2). The areas with medium and high values were located in Central Africa, the Great Lakes region in North America, the Alps, the Yenisei Basin, and Honshu

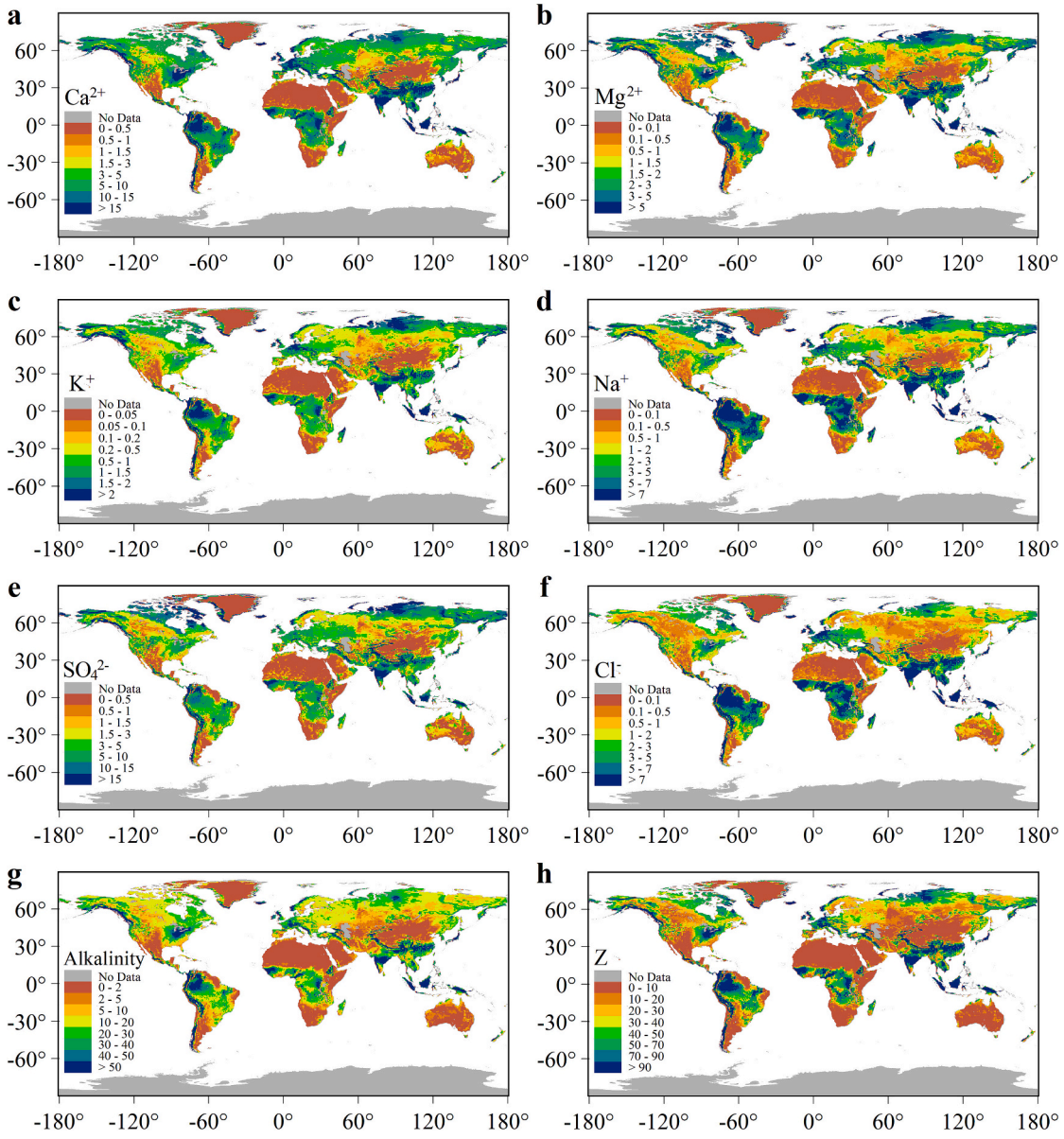

Fig. 2. Spatial distribution of the major ionic fluxes derived from the chemical weathering of rocks (ICWR) (Mg km^{-2} yr^{-1}). Z is the total content of the ICWR.

Island in Japan. According to the Köppen climate classification (Beck et al., 2020), most of these areas have tropical rainforest, tropical monsoon, savannah, Mediterranean, oceanic, and polar tundra climates. The areas with extremely low total ion fluxes were mainly located in the Sahara Desert, the Karahadi Basin, the Horn of Africa, the Arabian Peninsula, Southwest Asia, Central-Eastern Asia, the Greenland Island Ice Sheet, the Southwestern United States, Patagon, and Australia. Except for the Greenland Island Ice Sheet, these areas were roughly the same as the nine major arid and semi-arid regions in the world (Hulme, 1996). The above areas mainly have desert and polar frost climates.

The high-value areas of the ICWR and its total ion contents near the equator mostly occurred in high temperature, high precipitation, high evapotranspiration, and high runoff areas, while the high and middle values areas above 60° N had higher runoff values. All of the above climatic factors can promote the chemical weathering of rocks. There were more basalts with fast weathering rates distributed in the middle and high value areas. The low-value areas were located in arid areas with low rainfall, high evapotranspiration, and low runoff. This indicates that the spatial distribution of the ICWR flux was affected by a combination of factors. It exhibited the greatest correlation with the runoff distribution, and it was also closely related to factors such as rainfall, evapotranspiration, and lithology.

3.1.2. *Temporal variation in the ICWR in riverine transport*

Rock properties were a crucial factor affecting the magnitude of the ICWR. As can be seen from Fig. 3, the average annual total ICWR from 1980 to 2009 was $5.4{\cdot}10^9$ Mg yr^{-1}, of which cations accounted for 33% and anions accounted for 67%. For the ICWR, alkalinity accounted for 45%, Ca^{2+} accounted for 17%, SO_4^{2-} accounted for 14%, Na^+ accounted for 9%, Cl^- accounted for 8%, Mg^{2+} accounted for 6%, and K^+ accounted for 2%. The ICWR increased at a rate of $6.47{\cdot}10^6$ Mg yr^{-1} overall. Among them, Ca^{2+}, K^+, SO_4^{2-}, and alkalinity exhibited increasing trends, and the growth rate of alkalinity was the fastest, reaching $5.65{\cdot}10^6$ Mg yr^{-1}. K^+ had the slowest growth rate, and the growth rate of alkalinity was 2.63 times faster that of K^+. In contrast, Mg^{2+}, Na^+, and Cl^- exhibited decreasing trends. The rate of decrease of Cl^- was the fastest ($-5.16{\cdot}10^6$ Mg yr^{-1}), and it was 10.42 times that of Mg^{2+}, which had the slowest rate of decrease. The alkalinity changed the most rapidly because the weathering of carbonate rocks and silicate rocks both generate HCO_3^-, and carbonate rocks, which have a high

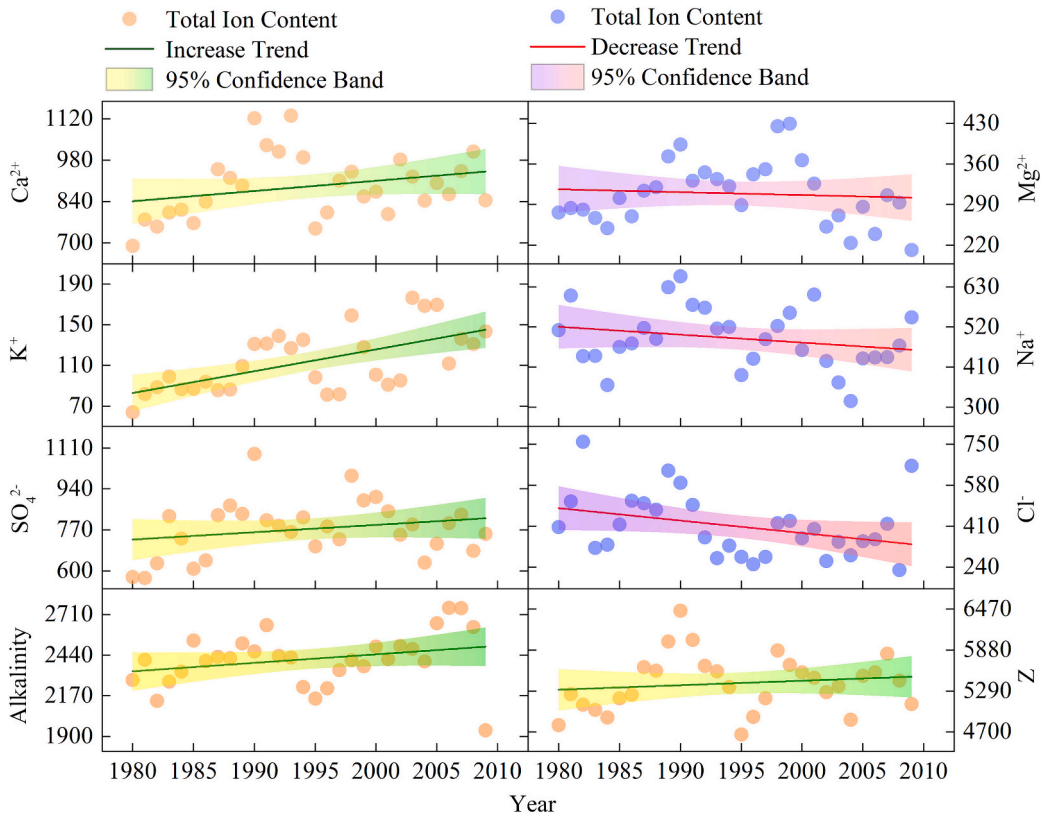

Fig. 3. Temporal variations in the total ICWR content (Mg yr^{-1}).

sensibility to climate change, are weathered faster. Mg^{2+} is mainly produced by the weathering of dolomite and silicate rocks, and the weathering of these two rock types is slow. The activity of Mg^{2+} was lower, so the change in Mg^{2+} was slower. This shows that the magnitude and rate of change of the ICWR were influenced by the lithology. Rocks with a faster weathering rate produced a larger number of ions, resulting in a faster rate of change, and vice versa.

Furthermore, the total ion content of the ICWR fluctuated greatly during the study period, with the maximum value occurring in 1990 and the minimum value occurring in 1995. The fluctuation ranges of the average annual total contents of the other major ions were different, but they all exhibited a peak around 1990 and a trough around 1995, indicating that the correlation between the interannual variability of the ICWR and its total ion contents.

3.1.3. *Spatial evolution of the ICWR in riverine transport*

Compared with the spatial distribution of each ion, its evolution trend was quite different. By analyzing the differences in the fluxes of the ICWR and its total ion contents (Fig. 4), it was found that the area in which SO_4^{2-} and K^+ increased was smaller than the area in which they decreased, exhibiting an increasing trend from 1980 to 2009. The area in which Cl^- decreased was smaller than the area in which it increased. The areas with obvious increasing Ca^{2+} fluxes included Southeast Asia, the southern part of the Yangtze River Basin, the Japanese archipelago, Western Europe, the eastern part of the Appalachian Mountains, northwestern South America, and other areas with high Ca^{2+} flux. There were also areas where the Ca^{2+} flux was high but exhibited a significant decreasing trend, including Southern Asia, the Western Siberian Plain, and the Labrador Plateau. The evolutionary distribution of SO_4^{2-} was roughly similar to that of Ca^{2+}. The differences were that the flux of SO_4^{2-} exhibited decreasing trends in the Amazon Plain and Western Europe, while the northern islands of North America and the coast of Siberia exhibited significant increasing trends. The evolutionary distribution of alkalinity was similar to that of Ca^{2+}, except for the fact that more regions in Central Africa and Southern Asia exhibited increasing trends. K^+ exhibited a significant decreasing trend in Central Europe, while the northern Rocky Mountains, coastal areas of Siberia, and Indonesia exhibited significant increasing trends. Cl^- and Mg^{2+} decreased significantly in Central Africa, northern South America, Southeast Asia, and Southern Asia. The decrease in Na^+ was the most significant in Southern Asia and Western Europe, while it increased in Southeast Asia.

The areas in which the ICWR's total ion flux decreased accounted for 49%, the areas in which it increased accounted for 46%, and the areas with stable trends accounted for 5%. The areas with the most significant decreasing trends were in Southern Asia and the Labrador Plateau. Most of the arid and semi-arid areas with extremely low ion fluxes exhibited slight decreasing trends. The areas with obvious increasing trends were the Japanese archipelago, Southeast Asia, the southern part of the Yangtze River Basin, the Western Cordillera, the Appalachian Mountains, and the Alps. In summary, the ions that exhibited decreasing trends in a large area may have exhibited an increasing trend in general, and the ions that exhibited increasing trends in a large area may have exhibited a decreasing trend in general. This shows that the change trends in the areas with high ion activity coefficients from 30° N to 30° S dominated the global variations in the different ions, including Southeast Asia, Southern Asia, the southern part of the Yangtze River Basin, and northwestern South America. These areas had high ionic activity coefficients (Lechuga-Crespo et al., 2020) due to factors such as high runoff (Fekete et al., 2002), tropical and temperate climates (Beck et al., 2020), and unique soil types (FAO et al., 2012).

3.2. *Impact of climate change on the ICWR from 1980 to 2009*

Chemical weathering of rocks had sensitive feedback on climate change, which in turn led to changes in the ICWR. Comparing the differences in the relative contributions of the eight selected factors representing climate change to the ICWR and its major ions revealed that Q

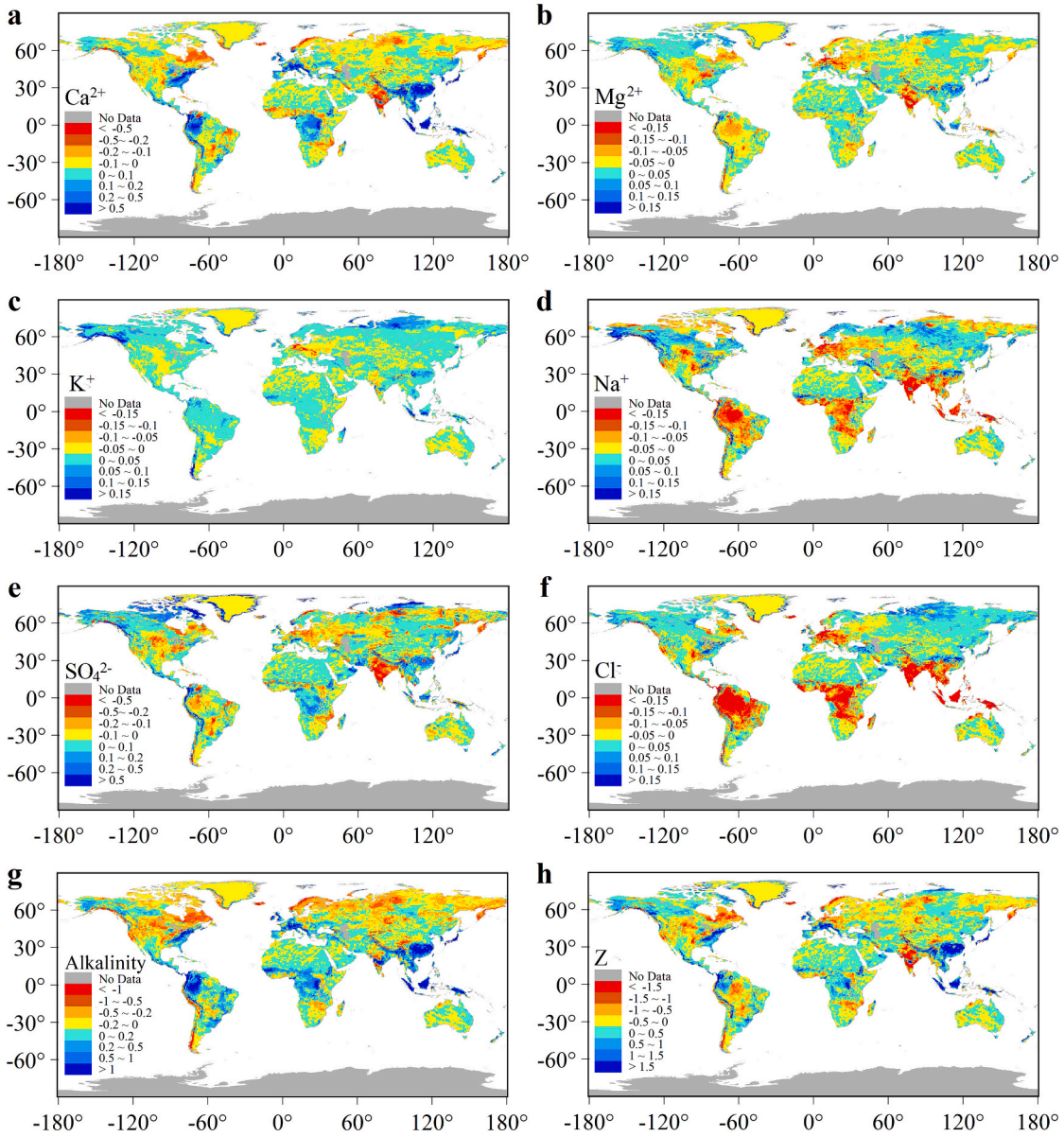

Fig. 4. Spatial evolution of the ICWR' fluxes (Mg km^{-2} yr^{-1}).

made the highest relative contribution to the ICWR (Fig. 5), and it made the highest relative contribution to Mg^{2+} (31%) and the lowest relative contribution to Cl^{-} (25%). Q was followed by ND, SM, and P, the relative contribution rates of which were >10%. The contributions of T and WS were the next lowest, with relative contribution rates of >9%. Finally, ET had a relative contribution rate of >6%, except for the smallest contribution rate of 4% to Mg^{2+}, and the relative contribution rate of PCO_2 was >5%. For the total ion content of the ICWR, the relative contribution rate of Q was also the largest. The contribution rates of ND, SM, and P were all >10%, and the contribution rates of the other factors were all >6%.

Thus, although the effects of the different climate change factors on the ICWR and its main ions were different, they were still proportionally related. Q had the greatest impact because the chemical weathering of rocks is greatly affected by runoff (Raymond, 2003; Raymond et al., 2008), and the ions in basins are also carried away by runoff. Thus, the runoff not only affected the total ion content, but it also affected the spatial distributions of the ions. The enhancement of the ND not only led to an increase in the exogenous acid in aquatic environments, but it also promoted the growth of plants. Both exogenous acids and the biochemical effects of plants have positive effects on the chemical weathering of rocks, which led to an increase in the total content of the ICWR in global riverine transport. SM, P, and T are also important factors affecting the chemical weathering of rocks. The WS changes the total ion content in a basin by affecting the physical weathering of rocks. The influence of ET on the ICWR was not significant because the impact of ET on the chemical weathering of rocks needs to be analyzed in combination with P since they influence the chemical weathering of rocks by jointly affecting the magnitude of Q. Among them, P increases Q, and ET decreases Q. Although the PCO_2 has a promoting effect on the chemical weathering of rocks, it should be considered in combination with other factors. Because PCO_2 will be diluted in areas with higher Q and P, the influence of Q and P will be more significant.

Based on the conclusion that ICWR showed an increasing trend during the study period, the different effects of the climate change factors on the major ions and their total contents in the ICWR indicate that the ICWR has positive feedback on climate change, and its response to changes in the water environment is the most significant. Because not only factors such as Q, SM, P, and ET directly affect the water environment, ND and PCO_2 also affect the water environment by changing

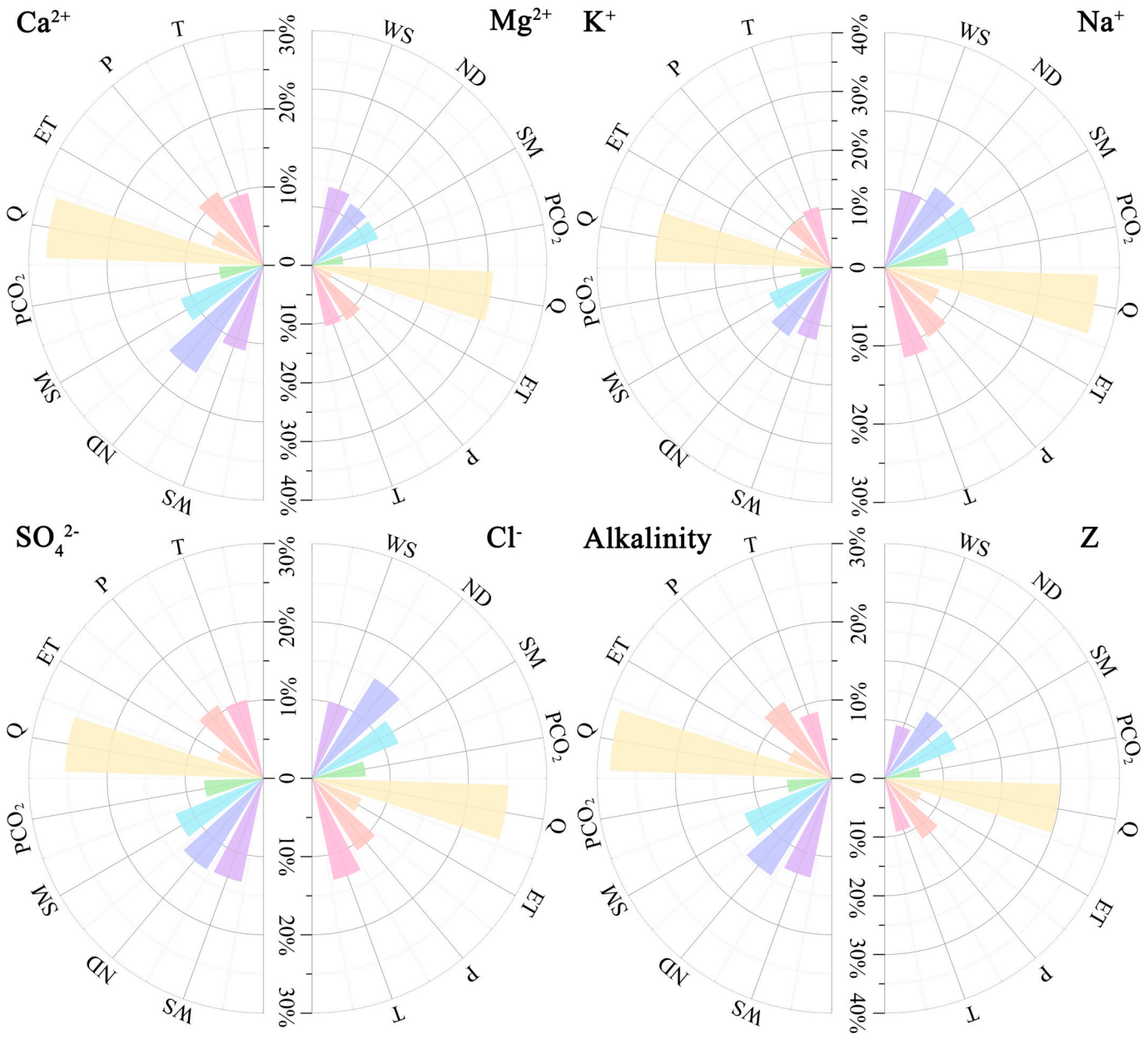

Fig. 5. Relative contribution rates of the factors affecting the ICWR. T: temperature; P: precipitation; ET: evapotranspiration; Q: runoff; PCO_2: partial pressure of carbon dioxide; SM: soil moisture; ND: nitrogen deposition; WS: wind speed.

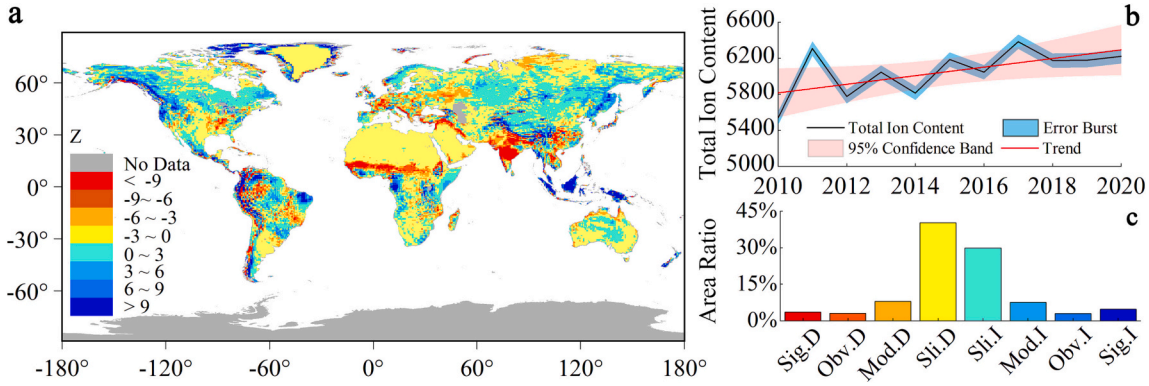

Fig. 6. Changes in the ICWR flux from 2010 to 2020. a: Spatial evolution of the ICWR (Mg km^{-2} yr^{-1}); b: Temporal variations in the ICWR (Mg yr^{-1}); c: Percentages of areas with different trends, Sig is significantly, Obv is obviously, Mod is moderately, Sli is slightly, D is decrease, and I is increase.

the pH value. T can accelerate the weathering rate of rocks, and it can also affect the water environment by changing the ET. Physical weathering can promote chemical weathering via the crushing of rocks. Thus, the influences of T and WS on the ICWR were also very important. Various factors influenced and interacted with each other, and together they had an impact on the ICWR. Therefore, climate change will inevitably lead to changes in the ICWR (Fig. S2).

3.3. Changes in the ICWR from 2010 to 2020

We estimated the ICWR from 2010 to 2020 using measured river hydrochemistry data from 1980 to 2009 and the evolutions of the influencing factors from 2010 to 2020 (Fig. 6). The results revealed that the ICWR maintained an increasing trend during 2010–2020 ($4.56{\cdot}10^{7}$ Mg yr^{-1}), which was seven times the increasing trend of the ICWR from 1980 to 2009. The ICWR has increased by 30% over the past 40 years, indicating that the total content of the ICWR will continue to increase under the persistent effects of global warming, and the increasing trend will be more significant (Fig. 6b). Compared with 1980–2009, the differences in the spatial trend of the ICWR were that the southern part of the Yangtze River Basin, the northern part of Southeast Asia, and the Japanese archipelago changed from a significant increasing trend to a decreasing trend. More areas in Africa, Europe, and central North America exhibited decreasing trends, with a decreasing trend evident in the southern part of the Sahara Desert (Fig. 6a). In 2010–2020, the area in which the ICWR exhibited a decreasing trend increased by 5% compared with 1980–2009 (Fig. 6c). Areas with slight changes accounted for as much as 70% of the total area, and areas with obvious changes accounted for only 14%, indicating that the areas with high ion activity coefficients between 30° N and 30° S still dominated the trend of the ICWR.

4. Discussion

4.1. Impact of ICWR on vegetation change

Comparison of Fig. 7 and Fig.S3 shows that the correlation and significance level of ICWR and NPP were higher than the correlation (Fig.

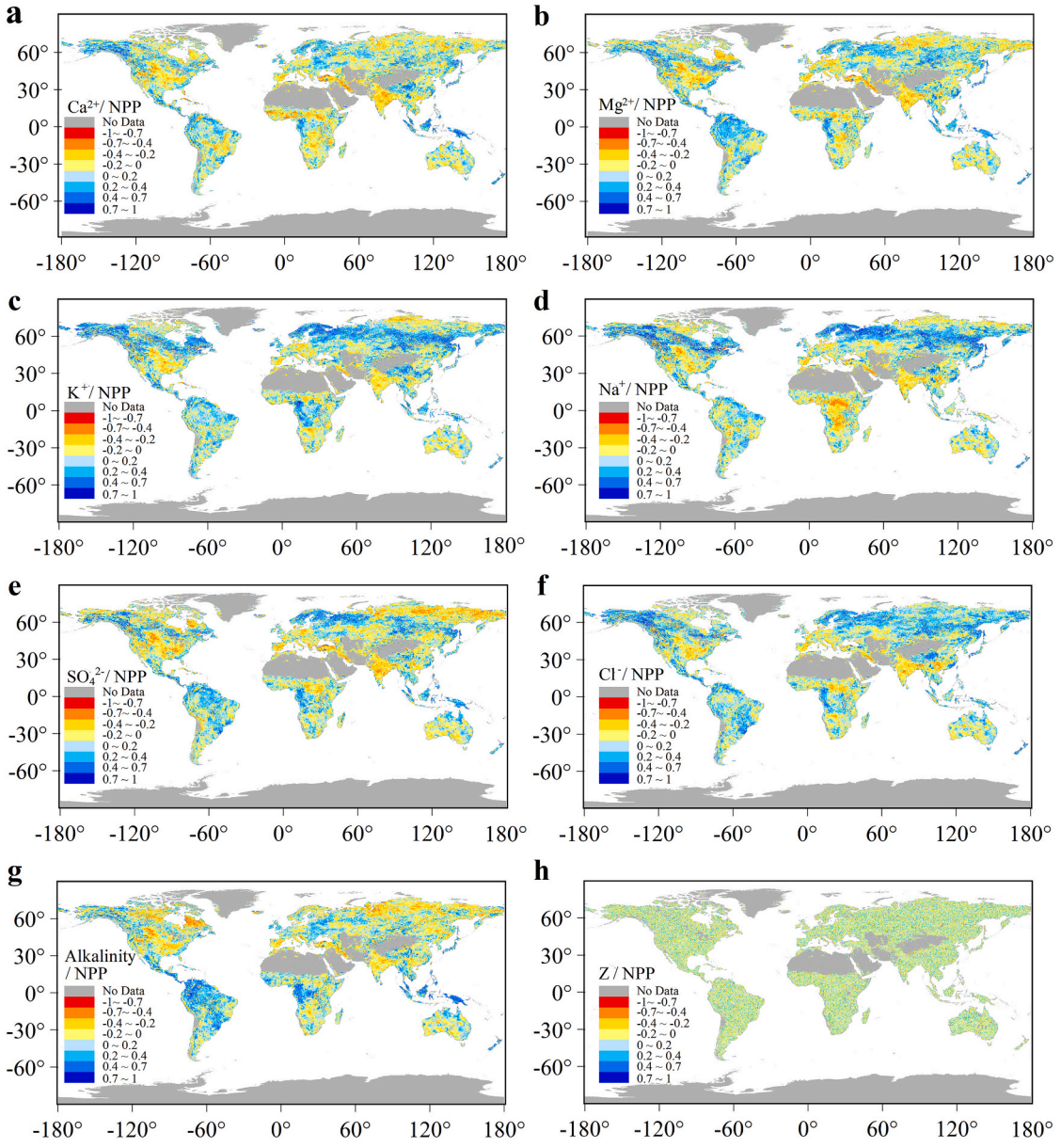

Fig. 7. Correlation of ICWR and its total ions with NPP.

S4) and significance level (Fig.S5) of ICWR and FVC. FVC can only describe the changes in the coverage area of the vegetation surface, while NPP is an index that can more accurately characterize plant activity variables, and has the characteristics of describing the relationship between plants and the external environment in energy transfer and material circulation. This indicates that the spatial distribution of the correlation between ICWR and NPP can more clearly represent the relationship between ICWR and vegetation and the effect of ICWR changes on the carbon sequestration capacity of ecosystems. The total ions of ICWR did not show a significant correlation with NPP (Fig. 7h), but rather the correlation of different major ions with ICWR respectively was more pronounced. At the same time, rock weathering is mainly influenced by changes in the water environment and is less sensitive to changes in vegetation (Gong et al., 2020). Therefore the correlation between ICWR and NPP was considered here as the effect of ICWR changes on NPP.

The positive correlation between Na^+ and NPP was the most obvious, and the areas where the correlation coefficient was >0.7 and the *p*-value was <0.01 were mainly located in northwestern North America and the plains of Eastern Europe to the Siberian plains, which belong to the continental humid climate. The Na^+ flux from rock weathering in these areas was low and showed a slight increase trend. As plants have a low and very strict sodium requirement, the appropriate increase in its concentration in the low value region of Na^+ can promote plant growth. The next most positively correlated ions with NPP were Cl^- and alkalinity, and the areas where they and other major ions had correlation coefficients >0.7 with NPP were located in northwestern South America and Southeast Asia, in addition to the above areas. Compared to the positive correlation between major ions and NPP, the negative correlation between the two was not significant. The few regions with correlation coefficients less than −0.7 were mainly located in northern North America. Calcium, magnesium, potassium, sodium, sulfur, and chloride are all essential elements for plant growth, and increased ICWR has a greater promotion than inhibition effect on vegetation growth. This indicates that an appropriate increase in ICWR can promote vegetation growth, but exceeding the threshold value of ions required for vegetation can have adverse effects on vegetation growth. In general, there were not many areas where the impact of ICWR on vegetation was significant. This is mainly because rivers contain ions from many other sources in addition to those produced by chemical weathering of rocks. And the vegetation is influenced not only by the ions in the river, but also by other climatic and ecohydrological factors. However, the ecological effects of increased ions in rivers caused by climate change still deserve our attention and investigation.

4.2. Accuracy assessment of the results

To verify the accuracy and reliability of our calculation results, we compared the relevant research results of previous scholars with the results of this study (Table 1). Our calculated ICWR was 48% higher than the average value of previous studies. This is mainly due to differences in the research periods, data sources, and research methods. First, we conducted the first long-term dynamic analysis of the ICWR compared to previous static studies, and we demonstrated that the impact of the ICWR on climate change is increasing, so this was the essential reason for our slightly higher results. Second, because of the significant influence of the water environment on the chemical weathering of rocks, the climate and hydrological conditions of the basins at a given time, especially runoff, are directly related to the ICWR. Both Meybeck and Probst's studies were based on watershed calculations before the 21st century, while this study was based on pixel calculations from 1980 to 2020. In addition, their research methods were different from those used in this study, and other reasons also caused differences in our results (Meybeck et al., 1979; Probst et al., 1992). Although our calculation method was the same as that of Lechuga-Crespo, due to the different data sources and influencing factors considered, our calculation results represent continuous changes over many years, and our results take into account the positive effects of climate change. Thus, our findings are slightly larger than the results he obtained (Lechuga-Crespo et al., 2020). The interference of human activity with the ICWR was considered in our data estimates because human interference generally aggravates the weathering of rocks and increases the ICWR. Recent research has shown that global fluxes of solutes to the oceans has improved the data accuracy and the interference of human activities, so the estimated result has increased by 68% compared with those of previous studies (Wu et al., 2021). The average R^2 of our simulations of ICWR using the Random Forest model was 0.71, indicating the high simulation ability of the model and further demonstrating the high accuracy and reliability of our results.

Previous studies have made great contributions to the calculation and distribution of the ICWR. Based on previous studies, in this study, we estimated the ICWR from 1980 to 2020 on grid cell scale. We conducted an in-depth analysis of its spatiotemporal evolution, explored the relative contribution rates of its major influencing factors, and clarified the change trend of the ICWR under climate change and the differences in the responses to different influencing factors. This research has important scientific significance for clarifying the dynamic changes in the global ICWR and its major ions in the long-term scale. By combining changes in ICWR with climate factors, this study not only examined the important role that ICWR play in responding to climate change and the range of ecological and environmental problems, but also explored the significant ecosystem impacts of the continuing role of climate change in increasing ICWR. The results also demonstrated the importance of the impact of chemical weathering of rocks on geochemical cycles.

4.3. Deficiencies and prospects

The river hydrochemistry database used in this study currently only contains data for the major ions measured at stations before 2010, so we studied the distribution and evolution of the ICWR in two stages. In the

Table 1
Comparison of the ICWR calculations in this study with those of other studies (10^6 Mg yr^{-1}).

Study	Meybeck (1979)	Probst (1992)	Lechuga-Crespo(2020)					This Study	
			M1	M2	M3	M4	M5	1980–2009	2010–2020
Ca^{2+}	502	510	374	484	428	527	477	892	912
Mg^{2+}	126	141	100	121	107	132	119	309	322
K^+	48	73	25	29	24	31	27	114	143
Na^+	129	211	223	202	176	221	202	489	555
SO_4^{2-}	307	355	401	500	465	545	490	774	847
Cl^-	215	223	246	263	221	287	241	410	584
Alkalinity	1940	2013	1815	2234	1954	2434	2139	2414	2698
Z+	868	935	722	836	734	911	825	1804	1932
Z-	1962	3046	2462	2997	2640	2640	3266	3598	4129
Z	3330	3981	3184	3833	3374	4177	3695	5402	6061

M1 ~ M5 represent the results obtained by 5 calculation models. Z+ represents the Ca^{2+}, Mg^{2+}, K^+, and Na^+. Z− represents the alkalinity, Cl^-, SO_4^{2-}.

years without measured data, the correlation coefficient model of the ions in the rivers and their influencing factors was established and the calculation results of the ions based on grid cell scale were obtained. Therefore, we only discussed the response and correlation of the ICWR to the climate change factors from 1980 to 2009. The inversion results obtained from the measured data were different from those obtained from the model, and the input factors used to establish the relationship were different, which will lead to different inversion results. In order to improve the accuracy of the calculation results, we optimized the model calculation.

After obtaining the inversion results for the river ions on grid cell scale, we calculated the ICWR using the equation for the soil shielding factor (Lechuga-Crespo et al., 2020). However, more studies on the ICWR are needed to compare and analyze the suitable equations. At present, few related studies have been conducted, and the soil shielding factors need to be updated and validated according to the existing data to improve their applicability in different regions. The promotion and use of the empirical model need to integrate the local actual situation and to fully consider the impacts of other factors. Therefore, the method of calculating the ICWR used in this study can be further verified and updated in future studies to improve the research on the ICWR and related aspects.

We selected eight representative factors to explore the impact of climate change on the ICWR and the relative contribution rates of the representative factors to the ICWR. However, it should be noted that other factors, such as vegetation coverage and human activities, also have an important impact on the ICWR. Since this article only considered the influences of natural factors such as meteorological and hydrological factors on the ICWR, the relative contribution rates of the influencing factors will differ from those obtained when more factors are considered. In future analysis of the factors influencing the ICWR, the impacts of other factors should be fully considered. And the eco-environmental effects caused by changes in the ICWR should be further explored, because ICWR not only affects the terrestrial ecology, but when it finally sinks into the ocean it may cause changes in the ocean pH, thus affecting the survival and reproduction of marine organisms.

Overall, through the above various improvement methods, we ensured the high reliability of the ICWR calculation results. The accuracy and time matching of the data we selected were high, and thus, more accurate calculation results were obtained. The research model in this study has important reference value for further improving the accurate estimation of the ICWR on the global scale in the future.

5. Conclusions

Our research demonstrates that climate change has significantly increased the positive contribution of the chemical weathering of rocks to the major ions in riverine transport. The average annual ICWR was $5.4{\cdot}10^{9}$ Mg yr^{-1} and increased at the rate of $6.47{\cdot}10^{6}$ Mg yr^{-1} from 1980 to 2009. The growth rate of the ICWR from 2010 to 2020 was seven times that during the previous 30 years. The major factors affecting the ICWR were runoff, nitrogen deposition, soil moisture, and rainfall, which had direct effects on the changes in the water environment. The soil environment, meteorological changes, and physical weathering could also cause changes in the ICWR. These factors increase the major ions in riverine transport by intensifying the chemical weathering of rocks. Under the continuous effects of climate change, the ICWR increased by 30% during the study period. The drastic global changes have led to significant changes in the ICWR, leading to more frequent exchanges in the exchange of ions between the land and sea and seriously affecting the stability of river and marine ecosystems and the evolution of organisms. Therefore, the impact of the continuous increases in the ion concentrations on the evolution of life and the various geochemical cycles will become an important direction for rock weathering research in the future.

Obviously, the weathering process of rocks has a non-negligible impact on the environment and ecosystem. The distribution and evolution of the ICWR are of great significance to gaining a comprehensive understanding of the global material cycle and the improvement of climate change research. We combined climate change with the chemical weathering of rocks, and we conclude that climate change has led to a significant increase in the major ions in riverine transport by intensifying the chemical weathering of rocks. And the increase of ICWR had a greater impact on vegetation carbon sequestration than its impact on vegetation cover changes, highlighting the important role of rock weathering in the global carbon cycle. This study clarifies the differences in the responses of the major ions in the ICWR to the different factors of climate change, has and the results of this study have a certain reference value for coping with global change and solving a series of eco-environmental problems caused by climate change.

Declaration of Competing Interest

The authors declare that they have no known competing financial interests or personal relationships that could have appeared to influence the work reported in this paper.

Data availability

The fundamental data used in our study is available in the public, and their websites are provided in “Materials and methods” section and other data are available from the corresponding author upon reasonable request.

Acknowledgments

This research work was supported by National Natural Science Foundation (No.U22A20619 & No.42077455), Western Light Cross-team Program of Chinese Academy of Sciences (No.xbzg-zdsys-202101), Strategic Priority Research Program of the Chinese Academy of Sciences (No.XDB40000000 & No.XDA23060100), Guizhou Provincial Science and Technology Projects (No.Qiankehe Support [2023] General 219 & [2023] Key 010), High-level Innovative Talents in Guizhou Province (No.GCC[2022]015-1 & No.2016-5648), Guizhou Provincial Science and Technology Subsidies (No.GZ2019SIG & No. GZ2020SIG).

Appendix A. Supplementary data

Supplementary data to this article can be found online at https://doi.org/10.1016/j.gloplacha.2023.104203.

References

Bai, X.Y., Zhang, S.R., Li, C.J., et al., 2023. A carbon neutrality capacity index for evaluating carbon sink contributions. Environ. Sci. Ecotechnol. 15, 100237.
Beaulieu, E., Godderis, Y., Donnadieu, Y., Labat, D., Roelandt, C., 2012. High sensitivity of the continental weathering carbon dioxide sinks to future climate change. Nat. Clim. Chang. 2, 346–349.
Beck, H.E., Zimmermann, N.E., McVicar, T.R., Vergopolan, N., Berg, A., Wood, E.F., 2020. Publisher Correction: present and future Köppen-Geiger climate classification maps at 1-km resolution. Sci. Data 7 (1).
Breiman, L., 1996. Bagging Preditors. Mach. Learn. 24 (2).
Breiman, L., 2001. Random Forests. Mach. Learn. 45 (1).
Cox, P.M., Betts, R., Jones, C.D., Spall, S.A., Totterdell, I.J., 2000. Acceleration of global warming due to carbon-cycle feedbacks in a coupled model. Nature. 408 (6813), 184–187.
Duan, Q.C., Zhang, B.F., 1992. Coefficient of partial correlation and its calculation. Chin. Q. J. Math. 7 (4), 6.
Fang, K.N., Jian-Bina, W.U., Zhu, J.P., Bang-Changa, S., 2011. A review of technologies on random forests. Stat. Inf. Forum 26 (03), 32–38.
FAO, IIASA, ISRIC, ISS-CAS, JRC, 2012. Harmonized World Soil Database. Version 1.2. FAO, Rome, Italy and IIASA, Laxenburg, Austria.
Fekete, B.M., Vörösmarty, C.J., Grabs, W., 2002. High-resolution fields of global runoff combining observed river discharge and simulated water balances. Glob. Biogeochem. Cycles 16 (3), 15-1-15-10.

Gaillardet, J., Dupre, B., Louvat, P., 1999. Global silicate weathering and CO_2 consumption rates deduced from the chemistry of large rivers. Chem. Geol. 159, 3–30.
Gibbs, R.J., 1970. Mechanisms controlling world water chemistry. Science. 170 (3962), 1088–1090.
Gislason, S.R., Arnorsson, S., Armannsson, H., 1996. Chemical weathering of basalt in Southwest Iceland: Effects of runoff, age of rocks and vegetative/glacial cover. Am. J. Sci. 296, 837–907.
Gong, S., Wang, S., Bai, X., Luo, G., Wu, L., Chen, F., Zeng, C., 2020. Response of the weathering carbon sink in terrestrial rocks to climate variables and ecological restoration in China. Sci. Total Environ. 750, 141525.
Hartmann, J., Moosdorf, N., 2012. The new global lithological map database GLiM: a representation of rorties at the Earth surface. Geochem. Geophys. Geosyst. 13 (12).
Hartmann, J., Lauerwald, R., Moosdorf, N., 2014. A brief overview of the global river chemistry database, GLORICH. Procedia Earth Planet. Sci. 10, 23–27.
Hawkesford, M., Horst, W., Kichey, T., Lambers, H., Schjoerring, J., Møller, I.S., White, P., 2012. Functions of Macronutrients. Marschner's Mineral Nutrition of Higher Plants 135–189.
Hindshaw, R.S., Tipper, E.T., Reynolds, B.C., Lemarchand, E., Bourdon, B., 2011. Hydrological control of stream water chemistry in a glacial catchment (damma glacier, Switzerland). Chem. Geol. 285 (1–4).
Hulme, M., 1996. Recent climatic change in the world's drylands. Geophys. Res. Lett. 23 (1), 61–64.
IPCC, 2018. Intergovernmental Panel on Climate Change Global Warming of 1.5°C, pp. 22–25.
Kemeny, P.C., Torres, M.A., Lamb, M.P., Webb, S.M., Dalleska, N., Cole, T., Fischer, W. W., 2021. Organic sulfur fluxes and geomorphic control of sulfur isotope ratios in rivers. Earth Planet. Sci. Lett. 562, 116838.
Lechuga-Crespo, J.L., Sánchez-Pérez, J.M., Sauvage, S., Hartmann, J., Suchet, P.A., Probst, J.L., Ruiz-Romera, E., 2020. A model for evaluating continental chemical weathering from riverine transports of dissolved major elements at a global scale. Glob. Planet. Chang. 192, 103226.
Li, H., Wang, S., Bai, X., Luo, W., Tang, H., Cao, Y., Wang, M., 2018. Spatiotemporal distribution and national measurement of the global carbonate carbon sink. Sci. Total Environ. 643, 157–170.
Li, C., Bai, X., Tan, Q., Luo, G., Wu, L., Chen, F., et al., 2022. High-resolution mapping of the global silicate weathering carbon sink and its long-term changes. Glob. Chang. Biol. 28 (14), 4377–4394.
Liu, J.K., Han, G.L., 2020. Major ions and δ34 SSO_4 in Jiulongjiang River water: investigating the relationships between natural chemical weathering and human perturbations. Sci. Total Environ. 724, 138208.
Liu, W., Xu, Z., Sun, H., Zhao, T., Shi, C., Liu, T., 2018. Geochemistry of the dissolved loads during high-flow season of rivers in the southeastern coastal region of China: anthropogenic impact on chemical weathering and carbon sequestration. Biogeosciences. 15 (16), 4955–4971.
Liu, W., Jiang, H., Guo, X., Li, Y., Xu, Z., 2022. Time-series monitoring of rive hydrochemistry and multiple isotope signals in the Yarlung Tsangpo River reveals a hydrological domination of fluvial nitrate fluxes in the Tibetan Plateau. Water Res. 225, 119098.
Liu, W., Xu, Z., Jiang, H., Zhou, X., Zhao, T., Li, Y., 2023. Lithological and glacial controls on sulfide weathering and the associated CO_2 budgets in the Tibetan Plateau: New constraints from small catchments. Geochim. Cosmochim. Acta 343, 341–352.
Luo, X.L., 2022. Particulate organic carbon exports from the terrestrial biosphere controlled by erosion. Catena. 209 (1), 105815.
Meybeck, M., 1979. Concentrations des eaux fluviales en éléments majeurs et apports en solution aux océans. Rev. Géol. Dynam. Géog. Phys. 21 (3), 215–246.
Meybeck, M., 2003. Global occurrence of major elements in Rivers. Treatise Geochem. 5, 207–223.
Moon, S., Huh, Y., Qin, J., Pho, N.V., 2007. Chemical weathering in the hong (red) river basin: rates of silicate weathering and their controlling factors. Geochim. Cosmochim. Acta 71 (6), 1411–1430.
National Climate Center, 2021. Blue Book on Climate Change in China. Science Press, Beijing.
Navarre-Sitchler, A., Thyne, G., 2007. Effects of carbon dioxide on mineral weathering rates at earth surface conditions. Chem. Geol. 243 (1–2), 53–63.
Patel, P., Raju, N.J., Subramanian, V., Gossel, W., Wycisk, P., 2020. Chemical weathering and atmospheric CO2 consumption in the semi-arid Swarnamukhi basin (Peninsular India) estimated from river water geochemistry. Appl. Geochem. 104520.
Probst, J.L., 1992. Géochimie et hydrologie de l'érosion continentale. Mécanismes, bilan global actuel et fluctuations au cours des 500 derniers millions d'années Université Louis-Pasteur, Strasbourg (Retrieved from).
Ran, C., Bai, X.Y., Tan, Q., Luo, G.J., et al., 2023. Threat of soil formation rate to health of karst ecosystem. Sci. Total Environ. 887, 163911.
Raymond, P.A., 2003. Increase in the export of alkalinity from North America's Largest River. Science. 301 (5629), 88–91.
Raymond, P.A., Oh, N.H., Turner, R.E., Broussard, W., 2008. Anthropogenically enhanced fluxes of water and carbon from the Mississippi River. Nature. 451 (7177), 449–452.
Relph, K.E., Stevenson, E.I., Turchyn, A.V., Antler, G., Bickle, M.J., Baronas, J.J., Tipper, E.T., 2021. Partitioning riverine sulfate sources using oxygen and sulfur isotopes: Implications for carbon budgets of large rivers. Earth Planet. Sci. Lett. 567, 116957.
Roy, S., Gaillardet, J., Allègre, C.J., 1999. Geochemistry of dissolved and suspended loads of the Seine River, France: anthropogenic impact, carbonate and silicate weathering. Geochim. Cosmochim. Acta 63 (9), 1277–1292.
Ruan, X., Yang, Y., Galy, A., Fang, X., Jin, Z., Zhang, F., Zhang, W., 2019. Evidence for early (≥12.7 Ma) eolian dust impact on river chemistry in the northeastern Tibetan Plateau. Earth Planet. Sci. Lett. 515, 79–89.
Sarin, M.M., Krishnaswami, S., 1984. Major ion chemistry of the Ganga–Brahmaputra river systems, India. Nature. 312 (5994), 538–541.
Sen, P.K., Lindeman, R.H., Merenda, P.F., Gold, R.Z., 1981. Introduction to bivariate and multivariate analysis. J. Am. Stat. Assoc. 76 (375), 752.
Sioli, H., 1968. Hydrochemistry and geology in the Brazilian Amazon region. Amazoniana. 1 (3), 267–277.
Stallard, R.F., Edmond, J.M., 1983. Geochemistry of the Amazon: 2. The influence of geology and weathering environment on the dissolved load. J. Geophys. Res. Oceans 88 (C14), 9671–9688.
Sun, Y.L., Guo, P., 2012. Spatiotemporal variation of vegetation coverage index in North China during the period from 1982 to 2006. Arid Zone Res. 29 (2), 187–193.
Tipper, E.T., Lemarchand, E., Hindshaw, R.S., Reynolds, B.C., Bourdon, B., 2012. Seasonal sensitivity of weathering processes: hints from magnesium isotopes in a glacial stream. Chem. Geol. 312-313, 80–92.
Ulrike, G., 2006. Relative importance for linear regression in R: the package relaimpo. J. Stat. Softw. 17, 1–27.
Vitousek, P.M., 1994. Beyond Global Warming: Ecology and Global Change. Ecology. 75 (7).
Walker, J.C., Hays, P.B., Kasting, J.F., 1981. A negative feedback mechanism for the long-term stabilization of Earth's surface temperature. J. Geophys. Res. 86, 9776–9978.
Wu, J., Xu, N., Wang, Y., 2021. Global syndromes induced by changes in solutes of the world's large rivers. Nat. Commun. 12, 5940.
Xi, H.P., Wang, S.J., Bai, X.Y., Tang, H., Luo, G.J., Li, H.W., Wu, L.H., Li, C.J., Chen, H., Ran, C., Luo, X.L., 2021. The responses of weathering carbon sink to eco-hydrological processes in global rocks. Sci. Total Environ. 788 (20), 147706.
Xiao, B.Q., Bai, X.Y., Zhao, C.W., Tan, Q., Li, Y.B., et al., 2023. Responses of carbon and water use efficiencies to climate and land use changes in China's karst areas. J. Hydrol. 617, 128968.
Xu, Y., Liu, W., Xu, B., Xu, Z., 2024. Riverine sulfate sources and behaviors in arid environment, Northwest China: Constraints from sulfur and oxygen isotopes. J. Environ. Sci. 137, 716–731.
Ye, R., Wright, A.L., Orem, W.H., McCray, J.M., 2010. Sulfur distribution and Transformations in Everglades Agricultural Area Soil as Influenced by Sulfur Amendment. Soil Sci. 175 (6), 263–269.
Zhang, Q.Q., Jin, Z.D., Zhang, F., 2015. Seasonal variation in river water chemistry of the middle reaches of the yellow river and its controlling factors. J. Geochem. Explor. 156 (3), 101–113.
Zhou, Y., Ju, W., Liu, Y., 2022. Characteristics and driving factors of global terrestrial ecosystem carbon fluxes from 1981 to 2019. Trans. Atmos. Sci. 45 (3), 332–344.